Efficient Adaptive Qualitative Methods for 3D Inverse Scattering Problems

Koung Hee Leem, Jun Liu, and George Pelekanos

Department of Mathematics and Statistics
Southern Illinois University Edwardsville, Edwardsville, IL 62026, USA
kleem@siue.edu, juliu@siue.edu, gpeleka@siue.edu

Abstract – In this paper we extend our recently developed 2D adaptive factorization method for efficiently solving 3D inverse acoustic and electromagnetic scattering problems. Different from the previously used Simpson rule, we propose to use Gaussian quadrature rule, which provides improved reconstruction quality. Several numerical examples are presented to illustrate the effectiveness of our proposed adaptive method. To achieve better efficiency and robustness, we have based our implementation on the existing adaptive quadrature codes.

Index Terms – adaptive Gaussian quadrature, factorization method, inverse scattering, linear sampling method.

I. INTRODUCTION

Inverse scattering problems [1] are of great importance in many fields of science and engineering, such as radar and sonar, medical imaging, and non-destructive testing. Efficient numerical algorithms for solving such nonlinear inverse problems have gained lots of recent attention, but the computational challenges remain for large-scale 3D applications. This paper is concerned with new efficient adaptive qualitative algorithms for solving 3D inverse scattering problems.

Depending on the amount of *a priori* knowledge of the physical properties of the underlying scatterer and the requirement of reconstruction quality in terms of resolution, current algorithms for inverse scattering problems can be roughly categorized into two groups: (i) *nonlinear optimization methods*, and (ii) *qualitative methods*. The nonlinear optimization methods [2–4] often involve an expensive iterative procedure, where a direct scattering problem needs to be (approximately) solved at each iteration. Although such optimization approaches require less number of incident fields, they do require *a priori* knowledge of the scatterer, such as boundary conditions (e.g, sound-soft or not) and its number of connected components, which may not be available in practice.

The established qualitative methods [5–7], including the linear sampling method [8] and the factorization method [9], have the key advantage of not requiring the aforementioned *a priori* information about the unknown scatterer. Moreover, qualitative methods were shown to be computationally parallelizable and faster than the nonlinear optimization methods. Nevertheless, the standard qualitative methods need to solve a large number of linear far-field equations over all sampling points of a possible very fine mesh over a large search domain, which can still be quite expensive in 3D applications involving large targets. Furthermore, qualitative methods often require a large amount of far-field measurements, although they can still deliver rough approximations with limited aperture data.

Within the framework of qualitative methods, many recent studies [10–12] have greatly improved the efficiency and applicability of the original linear sampling algorithm. In alignment with our proposed method, we point out that another adaptive scheme was proposed in [13], where only those coarse boundary cubes intersecting with a chosen cut-off plane is further subdivided into eight ($2 \times 2 \times 2$) sub-cubes. The multilevel linear sampling method (MLSM) [11] also demonstrates some local adaptive behavior by recursively labeling and removing non-boundary cells in different levels. However, the MLSM requires very careful numerical treatment on classifying all the square cells in order to avoid introducing breakage cells that should not be removed. We refer to [14] for a comparison between our adaptive factorization method and the MLSM in 2D cases. The more recently developed direct sampling methods [15, 16] have the benefit of using much less far-field data and avoiding directly solving ill-posed integral equations, which hence are more robust to data noise. Nevertheless, the mathematical foundation of such direct sampling methods is far less established.

We organize our paper as follows. In Section II, we briefly review the linear sampling and factorization methods. In Section III, based on adaptive Gaussian quadrature, we propose an adaptive factorization method that can automatically distribute more sampling points near the boundary of the scatterers. Section IV contains several numerical examples, which demonstrate the effectiveness of our proposed adaptive factorization method in comparison with the standard factorization method. Finally, some conclusions and remarks are given in Section V.

Submitted On: September 10, 2018
Accepted On: October 21, 2018

II. A REVIEW OF QUALITATIVE METHODS

In this section, following [1], we briefly describe the linear sampling and factorization methods for solving inverse acoustic obstacle scattering problems. For the purpose of exposition, we will only consider the scattering of a time harmonic acoustic wave by a bounded impenetrable sound-soft obstacle $D \subset \mathbb{R}^3$ and a C^2 boundary ∂D. Given an incident wave field u^i, its propagation against the obstacle D which is situated in a homogeneous medium will generate a scattered wave field u^s. Consider a time-harmonic plane wave $u^i(x) = e^{ikx\cdot\theta}$, where θ is the incident direction with $|\theta| = 1$ and $k > 0$ is the wave number. Let $u = u^i + u^s$ be the total field, which satisfies the following exterior Helmholtz equation:

$$\Delta u(x) + k^2 u(x) = 0, \quad x \in \mathbb{R}^3 \backslash \overline{D}, \tag{1}$$

subject to the Dirichlet boundary condition (sound-soft)

$$u = 0, \quad \text{on} \quad \partial D, \tag{2}$$

and the Sommerfeld radiation condition (with $r = |x|$)

$$\lim_{r\to\infty} r\left(\frac{\partial u^s}{\partial r} - iku^s\right) = 0. \tag{3}$$

The above direct obstacle scattering problem (1-3) has a unique solution $u \in C^2(\mathbb{R}^3\backslash\overline{D}) \bigcap C(\mathbb{R}^3\backslash D)$. In addition, the scattered field u^s has an asymptotic behavior:

$$u^s(x) = \frac{e^{ikr}}{r} u_\infty(\hat{x}, \theta) + O(r^{-2}),$$

as $r = |x| \to \infty$ uniformly in all directions, where $\hat{x} = x/|x|$ is the observation direction and u_∞ is called the far-field pattern of u^s. In general, the far-field pattern u_∞ also depends on the scatterer D and the wave number k.

The inverse obstacle scattering problem is then to determine the shape of D from many noisy far-field measurements $u_\infty(\hat{x}, \theta)$ for all $\hat{x}, \theta \in \mathbb{S}$ and a fixed $k > 0$. In other words, we need to invert the following abstract operator equation:

$$\mathscr{G}(\partial D) = u_\infty(\hat{x}, \theta), \quad \hat{x}, \theta \in \mathbb{S},$$

where the abstract operator $\mathscr{G}$ maps the boundary of the obstacle D to the corresponding far-field pattern for all pair of directions $(\hat{x}, \theta)$. This operator equation turns out to be highly nonlinear and severely ill-posed, which has been solved by Newton's method [2, 3], with the Fréchet derivative of $\mathscr{G}$ being inverted using Tikhonov regularization at each iteration. It is well-known that such nonlinear iterative methods are costly in practical computations and their effectiveness often depends on the faithfulness of the initial guess (i.e., a priori information) of the scatterer ∂D. In a typical setting, however, it is assumed that we know no or very limited information about the physical properties (i.e., sound-soft or penetrable) of the obstacle. Hence, the above mentioned linear sampling method [17] and its variants are widely used in practice, although they indeed have certain limitations [18, 19].

A. The linear sampling method

The linear sampling method (LSM) suggests to solve the following linear integral equation:

$$(Fg)(\hat{x}) = \Phi_\infty(\hat{x}, z) := \frac{1}{4\pi} e^{-ik\hat{x}\cdot z}, \quad z \in \mathbb{R}^3, \tag{4}$$

where the far-field operator $F : L^2(\mathbb{S}) \to L^2(\mathbb{S})$ is defined by:

$$(Fg)(\hat{x}) := \int_{\mathbb{S}} u_\infty(\hat{x}, d) g(d) ds(d),$$

and $\Phi_\infty(\hat{x}, z)$ is the far field pattern of the fundamental solution $\Phi(\cdot, z)$ of the Helmholtz equation. It was shown [5] that for every $\epsilon > 0$, there exists a function $g_z := g(\cdot, z) \in L^2(\mathbb{S})$ such that $\|Fg - \Phi_\infty\| < \epsilon$ and $\|g_z\|$ becomes unbounded as z approaches the boundary ∂D. Here $\|\cdot\|$ denotes the standard L^2 norm.

Based on this fact, the basic idea of the linear sampling method is to solve the above far-field equation (4) for each sampling point z of a uniformly spaced mesh grid in $\mathbb{R}^3$ containing D, and then plot a profile with the computed values of the indicator function $\|g_z\|$. The obstacle boundary ∂D can then be identified as the locus of those points z where $\|g_z\|$ changes sharply. However, a mathematical justification of such a linear sample method turns out to be nontrivial, since we in general do not have an explicit characterization of the range of the far field operator F. Such a theoretical gap, however, does not prevent its popularity and success in practice.

B. The factorization method

The factorization method (FM) [20], mainly as a mathematical improvement of the linear sampling method, provides an explicit and theoretically well-justified characterization for the support of a scattering object. It is based on the similar idea that a point $z \in \mathbb{R}^3$ belongs to the scatter D if and only if the test function $\Phi_\infty(\hat{x}, z)$ belongs to the range of a 'factorized' far-field operator. In particular, the FM approximately solves the following 'factorized' far-field equation:

$$((F^*F)^{1/4} g_z)(\hat{x}) = r_z(\hat{x}) := \Phi_\infty(\hat{x}, z),$$

by computing the norm of a possible solution g_z using Pickard's criterion for all sampling points z. Plotting of the values of these norms $\|g_z\|$ yields a profile of the scattering object, which allows us to identify the obstacle shape. For this purpose, we define the following continuous indicator function:

$$W_c(z) = \frac{1}{\|g_z\|}.$$

Then the FM is based on the following equivalence:

$$z \in D \Leftrightarrow r_z \in \text{Range}((F^*F)^{1/4}) \Leftrightarrow W_c(z)^{-1} < \infty.$$

In practical computations, one has to work with a finite dimensional approximation of the far-field operator F. Let F_n be the discretized far-field operator of dimension n that constructed by Nyström method [1], and its singular system is given by $\{\sigma_j, u_j, v_j\}_{j=1}^n$, where σ_j, u_j, and

v_j is the j-th singular value, left and right singular vector of F_n, respectively. In numerical implementations, we compute the corresponding discrete indicator function:

$$W_c(z) \approx W(z) := \left(\sum_{j=1}^{n} \frac{|v_j^{\intercal} r_z|}{\sigma_j} \right)^{-1}.$$

The standard FM then determines the shape of the scatterer D as the location of those points z where $W(z)$ becomes significantly large, since the corresponding series defining $\|g_z\|$ fails to converge whenever $z \notin D$. In a standard implementation, one has to compute $W(z)$ over a possibly very fine uniformly spaced mesh that adequately covers the search domain Ω. More specifically, the factorization method consists of four steps: *(1) Measure the far-field patterns $u_\infty(\hat{x}_j, \theta_i)$ for a sufficient number of different directions $\hat{x}_j$ and θ_i; (2) Select an estimated large search domain Ω covering D and discretize it with a fine uniform mesh $\mathcal{T}_h$; (3) Compute the indicator functional $W(z)$ for all sampling points $z \in \mathcal{T}_h$; (4) Plot the profile of $W(z)$ and determine D with a heuristic cut-off value $c > 0$.*

This straightforward sampling procedure, however, can be computationally very expensive, especially for those 3D applications involving large obstacles. For example, given an $N \times N \times N$ uniform mesh, the standard implementation needs to compute $W(z)$ at N^3 different sampling points, which hence has a time complexity of $O(N^3)$ if we treat the computation of each $\|g_z\|$ as one operation. In fact, compute each $\|g_z\|$ requires a matrix-vector product with $O(n^2)$ operations, if assuming the singular-value decomposition (SVD) of F_n has been computed (only once).

III. ADAPTIVE QUALITATIVE METHODS

In this section, we introduce an adaptive factorization method based on adaptive quadrature methods. The concept of adaptive discretization or adaptive mesh refinement has been well studied in scientific computing, such as in numerical integration [21] and adaptive finite element methods [22]. Adaptive quadrature has a long and very rich history with many slightly different versions, where the commonly used error estimate techniques are reviewed in [23].

The key idea behind an adaptive method is to adaptively allocate more grid (sampling) points to those regions where it becomes necessarily. Compared with the already established MLSM, our proposed adaptive factorization method (AFM) [14], based on adaptive global integration, has the advantage of better accuracy and robustness in the reconstruction of multiple obstacles and easier generalization to 3D problems. Furthermore, our AFM doesn't require selection of any cut-off values as in MLSM. The similar idea of adaptive allocation of unknowns/grid points (e.g., multi-resolution inversion) has also been widely discussed in microwave imaging [24–26].

Inspired by the fact that the indicator function $W_c(z)$ shows very sharp changes across the boundary of the obstacle domain, we propose to treat the indicator function $W_c : \mathbb{R}^3 \to \mathbb{R}_+$ as a function to be integrated over the global search domain Ω that contains the obstacle(s). To adaptively concentrate more sampling points near the unknown boundary ∂D of the obstacle D, we propose to utilize the efficient 3D adaptive Gaussian quadrature [27] to compute the 3D integration:

$$I(W_c) = \iiint_{\Omega} W_c(z)\, dV,$$

where $\Omega \subset \mathbb{R}^3$ is the estimated cube. The above integration is clearly well defined from the definition and boundedness of $W_c(z)$. It is important to mention here, that in our AFM, we are only interested in obtaining the adaptively generated quadrature points and use them as effective sampling points towards the reconstruction of the profile of the scatterer.

For simplicity, assume $\Omega = [-a, a]^3$. The standard m-point Gaussian(-Legendre) quadrature rule for approximating $I(W_c)$ reads:

$$I(W_c) \approx G_m(W) := \sum_{i=1}^{m} \sum_{j=1}^{m} \sum_{l=1}^{m} w_i w_j w_l W(x_i, y_j, z_l),$$

where $\{w_i, w_j, w_l\}$ are the Gaussian quadrature weights and $\{x_i, y_j, z_l\}$ are the Gaussian quadrature nodes. The above Gaussian quadrature rule is exact for multivariate polynomials of degree $2m - 1$ or less and is an accurate approximation when W_c can be well-approximated by multivariate polynomials.

Algorithm 1 AFM based on 3D Gaussian quadrature:
Initialization: $\Omega = [-a, a]^3, tol$
Output: A set of computed sampling points $\mathcal{A}$

procedure Q=AFM(Ω)
  $I_1 = G_5(W)$ over Ω
  $I_2 = G_8(W)$ over Ω
  Add new quadrature (sampling) points to $\mathcal{A}$
  if $|I_1 - I_2| < tol$ **then** ▷ Exit Recursion
    $Q = I_2$
  else ▷ Enter Recursion
    Divide Ω into eight subcubes $\{\Omega_j\}_{j=1}^{8}$
    For each Ω_j, compute Q_j =AFM(Ω_j)
    Add eight sub-integrals: $Q = \sum_{j=1}^{8} Q_j$
  end if
end procedure

The 3D adaptive Gaussian quadrature is based on the principle of divide and conquer, where each cube is recursively divided into eight ($2 \times 2 \times 2$) subcubes until the difference between two different quadrature approximations (e.g., G_5 and G_8, other combinations can also be used) for the integral over the same cube becomes

less than a user-supplied tolerance tol. Following [28, p. 358], our AFM algorithm is summarized in Algorithm 1, where we usually choose tol to be between 10^{-3} and 10^{-5} based on the domain size and scatterer shape.

With the set $\mathcal{A}$ of sampling points and indicator values computed by Algorithm 1, we can obtain a full-mesh profile via standard scattered data interpolation (i.e., the `scatteredInterpolant` function in MATLAB). The total computational cost (or maximum level of recursion) of the algorithm depends on tol and the shape of the indicator function W [14]. Due to the dramatic changes of W around the obstacle boundary ∂D, one would expect that more quadrature points are automatically clustered near the boundary, which therefore achieves the purpose of qualitatively reconstructing the obstacle boundary efficiently with less sampling points.

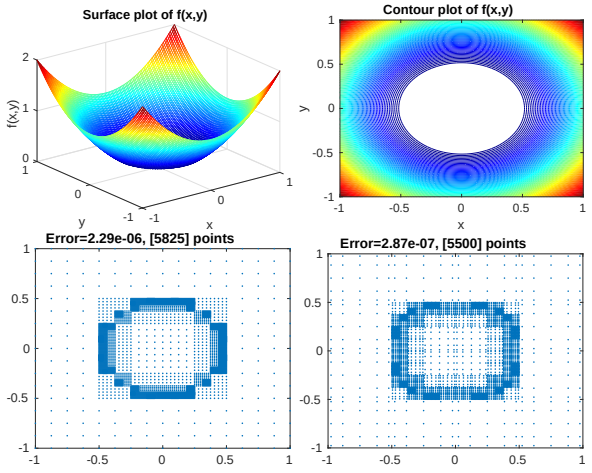

Fig. 1. Top: the surface (left) and contour (right) of a 2D indicator function $f(x,y) = (1/4 + (x^2+y^2))/2 + \sqrt{(1/4-(x^2+y^2))^2}/2$. Bottom: sampling points used by the adaptive Simpson quadrature (left) and the adaptive Gaussian quadrature (right), respectively.

For the sake of easier visualization, we first illustrate in Fig. 1 the distribution of the adaptively generated quadrature (sampling) points with a bowl-shaped 2D test indicator function, where both the 2D adaptive Simpson quadrature and Gaussian quadrature are tested. As expected, the adaptive Gaussian quadrature is more accurate (compare error) than adaptive Simpson quadrature. It is clear that more quadrature points are clustered along the inner circle that indicating sharp changes in function values. Similarly, we also plot in Fig. 2 the isosurface (with isovalue 0.5) and generated quadrature (sampling) points with a 3D test indicator function, where the generated Gaussian quadrature points closely track the function shape. Our AFM implementation is based on the well-tested adaptive Gaussian quadrature MATLAB codes developed in [27], which was shown to be very effective in treating functions with sharp gradients and cusps. Our main efforts lie in embedding the sampling procedure into this code to obtain an efficient implementation of AFM, without reinventing the wheels.

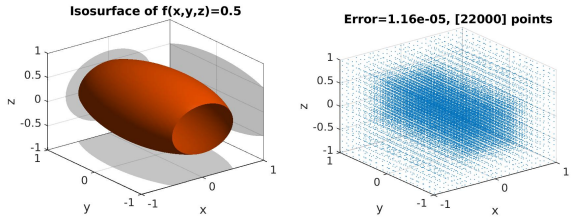

Fig. 2. The isosurface plot (left) of a 3D test indicator function $f(x,y,z) = (1/4 + (x^2 + y^2/4 + z^2))/2 + \sqrt{(1/4-(x^2+y^2/4+z^2))^2}/2$. The generated sampling points by the adaptive Gaussian quadrature (right).

IV. NUMERICAL RESULTS

In this section, we provide some numerical examples to demonstrate the effectiveness of our proposed AFM. All simulations are performed using MATLAB R2017b on a Dell Desktop PC with i7-7700K CPU@4.2GHz and 32GB RAM. The CPU time (in seconds) is estimated by timing functions *tic/toc*. The used far-field data are provided by the authors of the cited references, where they take n equidistantly distributed incident and observation directions on the unit sphere. To simulate noisy data, the discrete far-field matrix $F_n \in \mathbb{C}^{n\times n}$ is perturbed into $F_n^\delta = F_n + \epsilon(E_1 + iE_2).*F_n$, where E_1 and E_2 are two random matrices with entries uniformly distributed in $[-1,1]$. We choose $\epsilon = 10\%$ and denote $\delta := \|F_n - F_n^\delta\|_2$. For the standard FM, the Tikhonov regularization parameter is computed pointwisely using the `fzero` function at each sampling point via Morozonv's discrepancy principle [17], which costs about half of the total computation time. Inspired by the idea of one-shot regularization [29], in our AFM, we use a global regularization parameter that is estimated from the average of the 125 regularization parameters computed over a $5\times5\times5$ coarse mesh. The used isovalue γ for plotting isosurfaces is determined by the following global mean and standard deviation heuristic [30]:

$$\gamma = \text{mean}_{z\in\mathcal{T}_h}(W(z)) + 2\ \text{std}_{z\in\mathcal{T}_h}(W(z)).$$

A. Inverse acoustic scattering examples [31]

In Fig. 3, we plotted the reconstructed isosurfaces of four different shapes (acorn, cushion, and ellipsoid). Here we used a 258×258 far-field data with a $60\times60\times60$ sampling mesh points within a cube of size $[-1.5,1.5]^3$, where our AFM (with $tol = 10^{-3}$) is about 50–100 times faster than the standard FM (this can also be inferred by comparing the number of total sampling points). As we can observe, the reconstructed iso-surfaces by our AFM are hardly distinguishable from the standard FM, although they do have slightly rougher surfaces due to the used scattered interpolation (not counted into CPU

time) based on much less number of adaptively generated quadrature points. Notice the disconnected peanut shape is due to the over-estimated isovalue from large variation in the indicator function. The reconstruction quality of our AFM can be further improved if more sampling points are used by choosing a smaller tol.

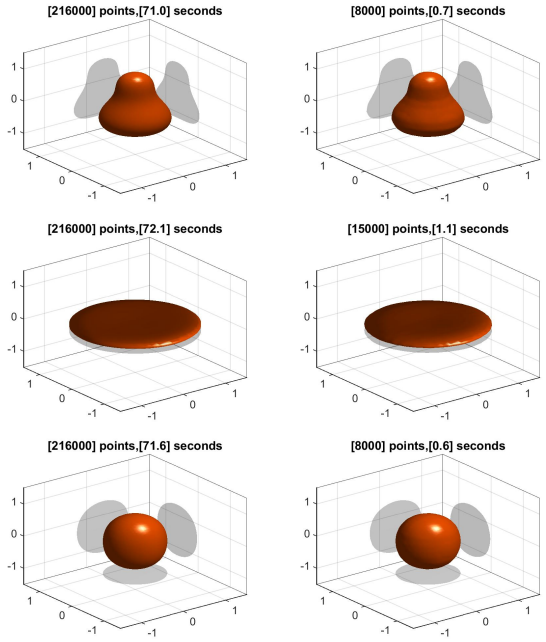

Fig. 3. Isosurfaces by the FM (left) and our AFM (right). From top to bottom: acorn, cushion, and ellipsoid shape.

B. Inverse electromagnetic scattering examples [5]

Due to limited space, we refer readers to [8] for the formulation of inverse electromagnetic scattering model and the corresponding linear sampling method. The application of our AFM to such problems is straightforward, but its overall computational cost becomes significantly higher due to expensive vector cross product operations. In Fig. 4 and Fig. 5, we plot the reconstructed isosurfaces of a teapot (with $k = 28, n = 252$ and a $50\times50\times50$ mesh within a cube of size $[-0.5, 0.5]^3$) and an aircraft (with $k = 4\pi, n = 252$ and a $80 \times 120 \times 160$ mesh within a box of size $[-1, 1] \times [-2, 2] \times [0, 4]$) by the standard FM and our AFM (with $tol = 10^{-4}$), respectively. Both scatterers have some very small detail feature that take more quadrature points to achieve a satisfactory resolution. In spite of some noticeable difference in detail feature, our AFM captures the major characteristics qualitatively and is significantly faster than the standard FM. The difference in size is due to slightly different regularization parameters and isovalues. The huge saving in computation time , or reduction in the total number of sampling points, makes our AFM very attractive to practical 3D applications.

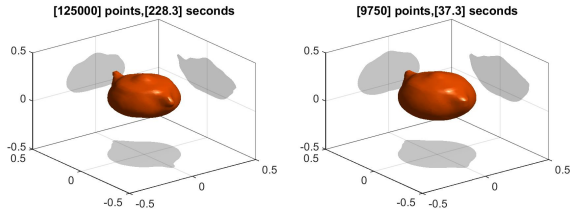

Fig. 4. Teapot by the FM (left) and our AFM (right).

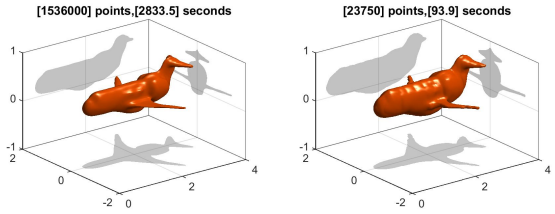

Fig. 5. Aircraft by the FM (left) and our AFM (right).

V. CONCLUSION

This paper presents an adaptive Gaussian quadrature based factorization method for solving 3D inverse obstacle scattering problems. It extends our previously developed 2D adaptive factorization method that was built upon 2D adaptive Simpson quadrature rule. With several benchmark inverse acoustic and electromagnetic scattering examples, the reported numerical results suggest our AFM achieves a dramatic improvement in the computational efficiency over the standard FM, while keeping a very satisfactory reconstruction quality.

One possible future work is to improve the computational efficiency of our AFM by using non-rectangular Gaussian quadrature rules to produce more irregular sampling points along a scatter of arbitrary shape.

REFERENCES

[1] D. Colton and R. Kress, *Inverse Acoustic and Electromagnetic Scattering Theory*, Springer New York, 2012.

[2] A. Roger, "Newton-Kantorovitch algorithm applied to an electromagnetic inverse problem," *IEEE Transactions on Antennas and Propagation*, vol. 29, no. 2, pp. 232–238, 1981.

[3] R. D. Murch, D. G. H. Tan, and D. J. N. Wall, "Newton-Kantorovich method applied to two-dimensional inverse scattering for an exterior Helmholtz problem," *Inverse Problems*, vol. 4, no. 4, pp. 1117–1128, 1988.

[4] G. Giorgi, M. Brignone, R. Aramini, and M. Piana, "Application of the inhomogeneous Lippmann–Schwinger equation to inverse scattering problems," *SIAM Journal on Applied Mathematics*, vol. 73, no. 1, pp. 212–231, 2013.

[5] D. Colton, H. Haddar, and M. Piana, "The linear sampling method in inverse electromagnetic scat-

tering theory," *Inverse Problems*, vol. 19, no. 6, pp. S105–S137, 2003.

[6] T. Arens and A. Lechleiter, "The linear sampling method revisited," *Journal of Integral Equations and Applications*, vol. 21, no. 2, pp. 179–202, 2009.

[7] F. Cakoni and D. Colton, *A Qualitative Approach to Inverse Scattering Theory*, Springer US, 2013.

[8] F. Cakoni, D. Colton, and P. Monk, *The Linear Sampling Method in Inverse Electromagnetic Scattering*, SIAM, Philadelphia, PA., 2011.

[9] A. Kirsch and N. Grinberg, *The Factorization Method for Inverse Problems*, Oxford University Press, Oxford, 2008.

[10] M. Brignone, G. Bozza, R. Aramini, M. Pastorino, and M. Piana, "A fully no-sampling formulation of the linear sampling method for three-dimensional inverse electromagnetic scattering problems," *Inverse Problems*, vol. 25, no. 1, p. 015014, 2008.

[11] J. Li, H. Liu, and J. Zou, "Multilevel linear sampling method for inverse scattering problems," *SIAM Journal on Scientific Computing*, vol. 30, no. 3, pp. 1228–1250, 2008.

[12] Y. Grisel, V. Mouysset, P. A. Mazet, and J. P. Raymond, "Adaptive refinement and selection process through defect localization for reconstructing an inhomogeneous refraction index," *Inverse Problems*, vol. 30, no. 7, p. 075003, 2014.

[13] D. Colton, K. Giebermann, and P. Monk, "A regularized sampling method for solving three-dimensional inverse scattering problems," *SIAM Journal on Scientific Computing*, vol. 21, no. 6, pp. 2316–2330, 2000.

[14] K. H. Leem, J. Liu, and G. Pelekanos, "An adaptive quadrature-based factorization method for inverse acoustic scattering problems," *Inverse Problems in Science and Engineering*, 2018, to appear. DOI:10.1080/17415977.2018.1459600.

[15] X. Liu, "A novel sampling method for multiple multiscale targets from scattering amplitudes at a fixed frequency," *Inverse Problems*, vol. 33, no. 8, p. 085011, 2017.

[16] K. H. Leem, J. Liu, and G. Pelekanos, "Two direct factorization methods for inverse scattering problems," *Inverse Problems*, vol. 34, no. 12, p. 125004, 2018.

[17] D. Colton, M. Piana, and R. Potthast, "A simple method using Morozov's discrepancy principle for solving inverse scattering problems," *Inverse Problems*, vol. 13, no. 6, pp. 1477–1493, 1997.

[18] A. G. Ramm and S. Gutman, "Analysis of a linear sampling method for identification of obstacles," *Acta Mathematicae Applicatae Sinica, English Series*, vol. 21, no. 3, pp. 399–404, 2005.

[19] A. Liseno and R. Pierri, "Shape reconstruction by the spectral data of the far-field operator: analysis and performances," *IEEE Transactions on Antennas and Propagation*, vol. 52, no. 3, pp. 899–903, 2004.

[20] A. Kirsch, "Characterization of the shape of a scattering obstacle using the spectral data of the far field operator," *Inverse Problems*, vol. 14, no. 6, pp. 1489–1512, 1998.

[21] W. Gander and W. Gautschi, "Adaptive quadrature—Revisited," *BIT Numerical Mathematics*, vol. 40, no. 1, pp. 84–101, Mar 2000.

[22] L. Beilina, M. V. Klibanov, and M. Y. Kokurin, "Adaptivity with relaxation for ill-posed problems and global convergence for a coefficient inverse problem," *Journal of Mathematical Sciences*, vol. 167, no. 3, pp. 279–325, 2010.

[23] P. Gonnet, "A review of error estimation in adaptive quadrature," *ACM Computing Surveys*, vol. 44, no. 4, pp. 1–36, 2012.

[24] S. Caorsi, M. Donelli, D. Franceschini, and A. Massa, "A new methodology based on an iterative multiscaling for microwave imaging," *IEEE Transactions on Microwave Theory and Techniques*, vol. 51, no. 4, pp. 1162–1173, 2003.

[25] X. Ye, L. Poli, G. Oliveri, Y. Zhong, K. Agarwal, A. Massa, and X. Chen, "Multi-resolution subspace-based optimization method for solving three-dimensional inverse scattering problems," *Journal of the Optical Society of America A*, vol. 32, no. 11, p. 2218, 2015.

[26] N. Anselmi, L. Poli, G. Oliveri, and A. Massa, "Iterative multiresolution bayesian CS for microwave imaging," *IEEE Transactions on Antennas and Propagation*, vol. 66, no. 7, pp. 3665–3677, 2018.

[27] S. Mousavi, J. Pask, and N. Sukumar, "Efficient adaptive integration of functions with sharp gradients and cusps in n-dimensional parallelepipeds," *International Journal for Numerical Methods in Engineering*, vol. 91, no. 4, pp. 343–357, 2012.

[28] M. Heath, *Scientific Computing: An Introductory Survey*, McGraw-Hill, 2002.

[29] R. Aramini, M. Brignone, and M. Piana, "The linear sampling method without sampling," *Inverse Problems*, vol. 22, no. 6, pp. 2237–2254, 2006.

[30] M. Fares, S. Gratton, and P. L. Toint, "SVD-tail: a new linear-sampling reconstruction method for inverse scattering problems," *Inverse Problems*, vol. 25, no. 9, p. 095013, 2009.

[31] K. A. Anagnostopoulos, A. Charalambopoulos, and A. Kleefeld, "The factorization method for the acoustic transmission problem," *Inverse Problems*, vol. 29, no. 11, p. 115015, 2013.